Significantly improved high-temperature energy storage performance of commercial BOPP films by utilizing ultraviolet grafting modification

Qingguo Chi[1,2], Tianqi Wang[1,2], Changhai Zhang[1,2], Hainan Yu[1,2], Xindong Zhao[1,2], Xu Yang[1,2], Qingquan Lei[1,2], Hong Zhao[1,2] ✉ and Tiandong Zhang[1,2] ✉

ABSTRACT

Commercial biaxially oriented polypropylene (BOPP) film capacitors have been widely applied in the fields of electrical and electronic engineering. However, due to the sharp increase in electrical conduction loss as the temperature rises, the energy storage performance of BOPP films seriously degrades at elevated temperatures. In this study, the grafting modification method is facile and suitable for large-scale industrial manufacturing and has been proposed to increase the high-temperature energy storage performance of commercial BOPP films for the first time. Specifically, acrylic acid (AA) as a polar organic molecular is used to graft onto the surface of commercial BOPP films by using ultraviolet irradiation (abbreviated as BOPP−AA). The results demonstrate that the AA grafting modification not only slightly increases the dielectric constant, but also significantly reduces the leakage current density at high-temperature, greatly improving the high-temperature energy storage performance. The modified BOPP−AA films display a discharged energy density of 1.32 J/cm³ with an efficiency of >90% at 370 kV/mm and 125 °C, which is 474% higher than that of the pristine BOPP films. This work manifests that utilizing ultraviolet grafting modification is a very efficient way to improve the high-temperature energy storage performance of commercial BOPP films as well as provides a hitherto unexplored opportunity for large-scalable production applications.

KEYWORDS

Capacitors, BOPP, ultraviolet irradiation, graft modification, energy storage.

1 Introduction

Polymer-based dielectric capacitors are widely used in energy storage and power conversion, such as high voltage direct current transmission, renewable-energy generating, and hybrid electric vehicle driving. With the continuous improvement of voltage levels and the thirsty demand for miniaturization of power devices, manufacturing advanced metallized film capacitors with excellent energy storage performance has attracted increasing attention[1]. However, the current polymer dielectrics are unable to meet the high-temperature requirements because of the sharp increase in electrical conduction loss in the capacitor films[2]. For example, while the near-engine-temperature in electric vehicles can reach above 120 °C, the upper operating temperature of commercial BOPP films is below 105 °C, so the redundant cooling device is required for lowering the capacitor's temperature[3–4]. Besides, the energy storage density of BOPP films is only 2–4 J/cm³ at room temperature due to its low dielectric constant (ε_r~2.2), and even decreases to 0.5 J/cm³ under high temperature and high electric field. Therefore, the capacitors have to be a large volume to meet the energy conversion requirements. In hybrid electric vehicles, the volume and cost of BOPP film capacitors are about 35% and 40% of that of power inverters, respectively, resulting in a large waste of space and cost[5]. So it is urgent to find an efficient way to improve the high-temperature energy storage performance of commercial BOPP films.

In recent years, it has become clear that the significant increase in the electrical conduction loss is the main bottleneck that results in the serious degradation of energy storage performance at elevated temperature, and numerous modification methods have been conducted to improve the energy storage performance. Doping inorganic fillers or coating inorganic barrier layers are two representative methods[6–8]. It was reported that the nanoparticle/polymer interface creates deep traps that slow down carrier transit, limit conduction current, and reduce energy loss. For example, Tian[9] prepared Al_2O_3/$BaTiO_3$/PP films and its dielectric constant was about 18, but the breakdown field strength decreased to 47.35 kV/mm, and the energy storage density of Al_2O_3/$BaTiO_3$/PP films was only 0.18 J/cm³. The incorporation of the inorganic nanoparticle is highly dependent on their compatibility and dispersion in the polymer matrix[10–12], the poor compatibility would counteract the modification effectiveness and even degrade the dielectric properties. Therefore, surface functionalization is required to improve the interfacial quality that can increase the compatibility of inorganic fillers and polymer matrix[13,14]. Zheng[15] prepared the core-shell nanoparticles by coating an organic rubber shell layer on the $BaTiO_3$ surface. Comparing to the pristine PP films, the dielectric constant of $BaTiO_3$/PP films increased to 5.8 while the dielectric loss changed slightly. The maximum energy density of 3.06 J/cm³ and the optimal breakdown strength of 370 kV/mm were obtained. The above mentioned modification approaches are used

to inhibit the charge transport inside the polymer films, some other methods are committed to impeding the charge injection from metal electrodes and reducing the electrical conduction loss[16]. Li reported that using plasma accelerated chemical vapor deposition to coat a SiO_2 barrier layer on the surface of BOPP films, the breakdown strength increased to 584 kV/mm and the highest energy density was 1.33 J/cm³ even at 125 °C. However, the interfacial quality between the inorganic barrier layer and the polymer films may be still a severe issue, particularly during the rolling procedure in capacitor manufacturing.

In this study, we proposed an organic grafting modification method to improve the high-temperature performance of BOPP capacitor films. To the best of our knowledge, it is the first time to utilize ultraviolet (UV) irradiation to realize the rapid grafting modification of acrylic acid (AA) onto the surface of BOPP films (abbreviated as BOPP–AA). The surface grafting structure provides deep chemical traps to suppress the charge injection from metal electrodes under high temperatures and high electric fields. Thus a highly excellent energy storage performance is successfully achieved at an ultra-high temperature of 125 °C for the BOPP–AA films, exhibiting a discharged energy density of 1.32 J/cm³ with an efficiency of >90%, which is 474% higher than that of pristine BOPP films.

2 Results and discussion

2.1 UV irradiation grafting modification

The commercial BOPP films have low dielectric constant due to the high regularity of the chemical chain, which results in low polarization under an electric field. However, the hydrogen on the tertiary carbon in the molecular chains looks considerably active,

which can be easily replaced by the extraneous functional group for grafting modification. In recent years, AA has become one of the most extensively used grafting solvents for enhancing the electrical properties of polymer materials. According to the independent gradient model simulation (IGM) results, it can be discovered that the intermolecular repulsion increases and charge transfer are considerably harder for AA grafts on BOPP molecular chains compared to that of pristine BOPP, as shown in Figure 1(a). Furthermore, AA comprises carbonyl and hydroxyl groups with high polarity, which is in favor of achieving a more stable grafting structure and electrical performance. The main chemical reaction of the grafting procedures is given in Figure 1(b). In this grafting reaction, the photoinitiator benzophenone (BP) can be excited to singlet excited states by UV irradiation, and then change into the triplet state via intersystem crossing transformation. This process can make the AA sensitize in the triplet state that easily reacts with the BOPP molecular chain to generate AA-free radicals and BOPP-free radicals. The above mentioned steps are the dominant reaction channels. Then, the AA-free radical and BOPP-free radicals would interact to form AA graft BOPP[17–19]. Figure 1(c) shows the schematic of the main equipment and grafting methods. To the best of our knowledge, it is the first time utilizing UV irradiation realized the rapid grafting modification of AA on the BOPP films. To remove the influence of the above factors on the grafting modification, we added a group of control trials during the experimental procedures. Figure S1 shows the dielectric constant at room temperature and the energy storage characteristics of UV irradiated films at 125 °C.

2.2 Structural characterization of the BOPP–AA films

Intrinsically, AA grafting modification is a surface engineering method, thus, it is essential to characterize the surface
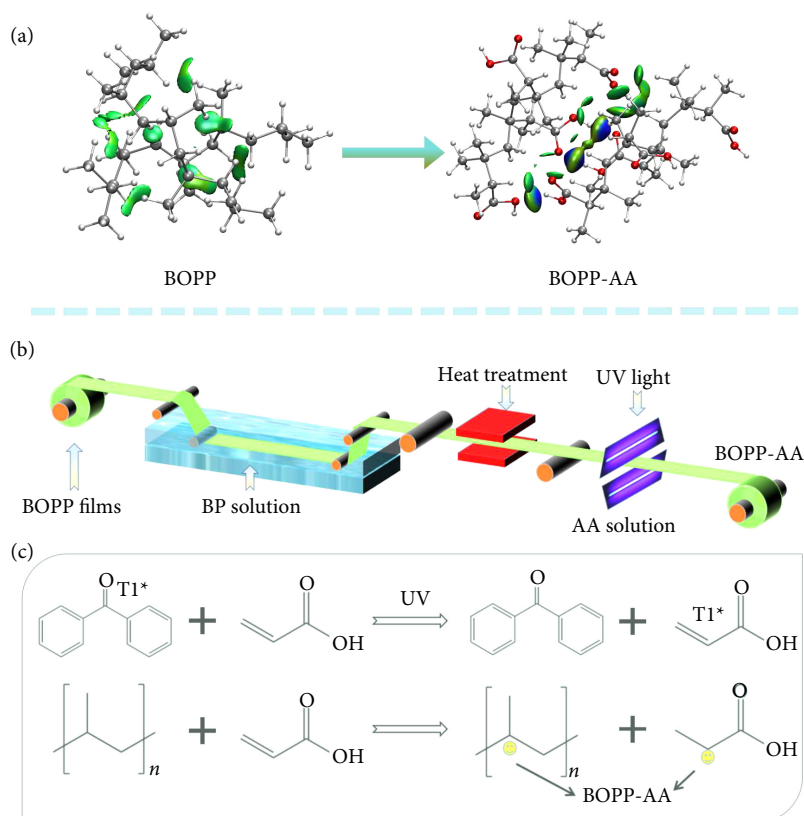

Fig. 1 **(a)** IGM simulation of BOPP and BOPP–AA. **(b)** Schematic diagram of the grafting process. **(c)** Molecular reaction formula during the grafting procedures.

microstructure of the BOPP–AA films with different UV irradiation times. Figure 2 illustrates the surface morphology and water contact angle of the resultant films. The surface roughness values are 4.91, 5.70, 6.17, and 8.46 nm for BOPP, BOPP–AA-1, BOPP–AA-5, and BOPP–AA-10 films, respectively, as shown in Figures 2(a)–2(d), indicating that the AA grafting modification increases the surface roughness of commercial BOPP films. As shown in Figures 2(e)–2(h), the water contact angle can also reflect the changes in the surface roughness of BOPP films after grafting modification. Generally, the increase in the surface roughness can enhance the hydrophobicity of the film's surface according to Cassie's theory, because there may be a groove structure in the rough surface that the air can be trapped in each groove, resulting in air retention in the concave part of the surface and hydropohobicity[20]. However, the water contact angle falls from 103.08° to 88.65° as the irradiation time increases, indicating the BOPP films become hydrophilic due to the carbonyl group after the grafting process.

As illustrated in Figure 3(a), X-ray photoelectron spectroscopy (XPS) results demonstrate that the content of oxygen elements in the BOPP–AA films increases as the UV irradiation time increases, meaning the increase in AA grafting content. To further confirm the chemical bond information, Fourier Transform infrared spectroscopy (FTIR) results are also provided in Figure 3(b). The carbonyl and hydroxyl groups at 1705 cm^{-1} and 3332 cm^{-1} can be detected in the BOPP-AA grafted films, as well as a small amount of unsaturated C–H bonds at 3085 cm^{-1}, confirming the effective grafting modification[21–23]. The carbonyl double bond of photoinitiator BP will be broken after UV irradiation, which can capture the hydrogen of tertiary carbon in the molecular of BOPP films, increase the unsaturated C–H bond of BOPP, and then graft with AA. The absorption peaks of C=O, O–H, and unsaturated hydrocarbon progressively rise with increasing irradiation time, showing the grafting AA content on the surface of BOPP films increases.

The melt crystallization curves of the BOPP–AA films were measured by differential scanning calorimetry (DSC), as shown in Figure 3(c). As UV irradiation induces the hydrogen on BOPP tertiary carbon to break off, the carbon-carbon bonds on BOPP tertiary carbon are progressively weakened as the irradiation time increases, leading to a decreased melting point. The gel permeation chromatography (GPC) demonstrates a slight decrease in the molecular weight distribution, which also indicates the occurrence of a broken chemical bond induced by the UV irradiation grafting

modification, as shown in Figure S2. The crystallization of BOPP films is characterized by X-ray diffraction (XRD), as shown in Figure 3(d). With the increasing temperature, it can be seen that the diffraction peak position shifts to a lower 2θ degree, and the peak intensity becomes considerably weaker. According to the Bragg diffraction equation of 2dsinθ = nλ, it can be deduced that the interplanar spacing of the molecular chains increases and the crystallization degrades with increasing temperature[24]. The changing trend of the BOPP–AA films is identical to that of pristine BOPP films, indicating that AA grafting has no discernible deleterious effect on the crystallization of the BOPP films. According to the above analyses, it can be deduced that the thermally-induced microstructure instability would not occur even if the temperature reaches 140 °C.

2.3　Dielectric properties of the BOPP–AA films

The dielectric parameters including dielectric constant and electric breakdown strength are crucial to the energy storage performance. Figures 4(a) and 4(b) indicate the dielectric constant and dielectric loss of the BOPP–AA films measured at selected temperatures and frequencies. The dielectric constant of pristine BOPP films (ε_r~2.2) is essentially stable from 1 Hz to 1 MHz, the low dielectric constant is due to molecule chain symmetry. For BOPP–AA films, the dielectric constant is slightly higher than pristine BOPP films, which increases from 2.26 to 2.42 at 25 °C and 10 Hz. The introduction of polar groups, such as C=O and O–H on the surface of BOPP films, improves the polarization and leads to an increase in the dielectric constant[25–28]. Furthermore, the side groups of BOPP films are readily detached from the molecular chains after the UV irradiation treatment, especially as the UV irradiation period increases results in the increased dielectric constant, as seen in Figure S3. The dielectric loss slightly increases with the extension of UV irradiation time, because UV radiation makes BOPP molecular chain and chemical bond break, which may produce considerably more polar end groups and lead to the increased polarization loss. The molecular vibration of the modified BOPP–AA films becomes remarkable at 125 °C, resulting in a sharp increase in dielectric loss in the high-frequency region.

The Weibull distribution of DC breakdown strength at different temperatures was measured and the results are given in Figures 4(c) and 4(d) and Figure S4. The breakdown strength of the BOPP–AA films is significantly enhanced compared to pristine BOPP films, for example, the breakdown strength of the
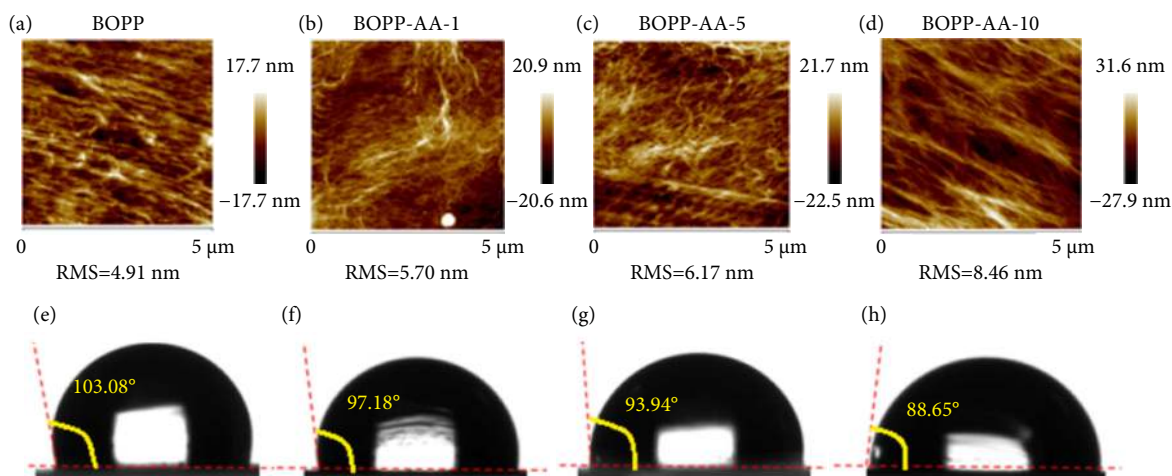

(a) BOPP	(b) BOPP-AA-1	(c) BOPP-AA-5	(d) BOPP-AA-10
RMS=4.91 nm	RMS=5.70 nm	RMS=6.17 nm	RMS=8.46 nm
(e) 103.08°	(f) 97.18°	(g) 93.94°	(h) 88.65°

Fig. 2　Surface microstructure characterization using atomic force microscopy and water contact angles. (a, e) BOPP. **(b, f)** BOPP–AA-1. **(c, g)** BOPP–AA-5. **(d, h)** BOPP–AA-10.
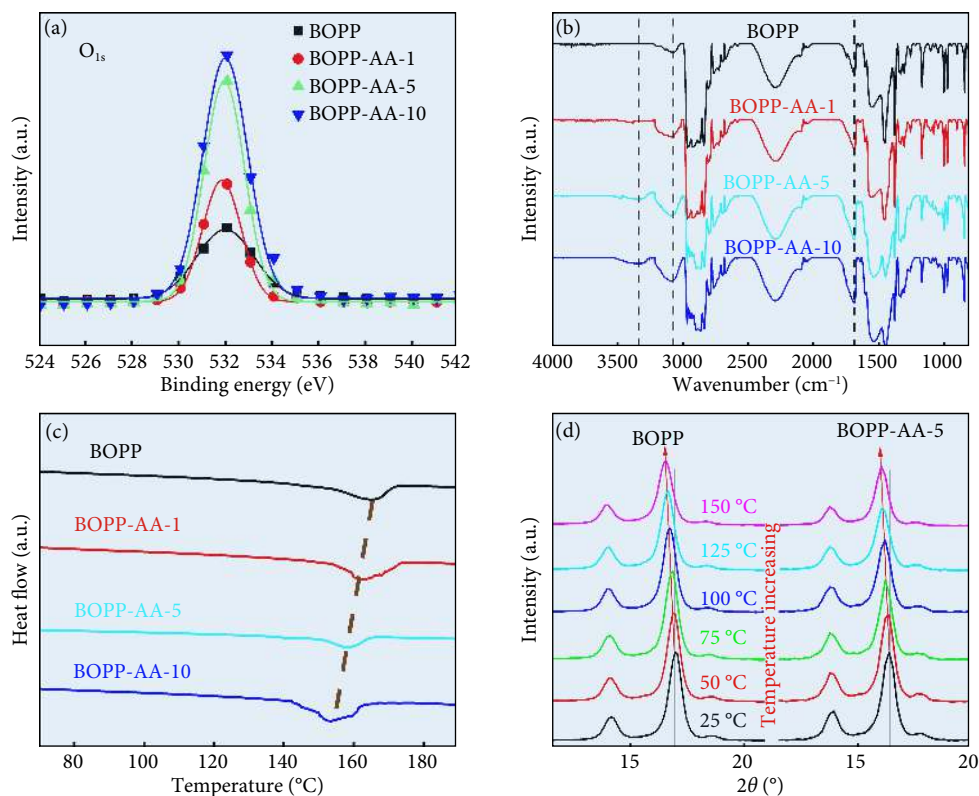
Fig. 3 Microstructure of the BOPP–AA films. (a) XPS, **(b)** FTIR, and **(c)** DSC. **(d)** XRD at different temperatures of BOPP and BOPP–AA-5.

BOPP–AA-5 films improves from 493.2 to 532.1 kV/mm at 125 °C. With the increase of the irradiation time, the breakdown field strength initially increases and subsequently decreases. This might be because the polar groups generated by UV irradiation grafting reaction can serve as electric charge traps, limiting carrier movement and reducing conductance loss[27]. For the BOPP–AA-5 films, the UV irradiation time may be sufficient to separate the side group from the molecular chains and break the chemical bond. However, with a further increase in irradiation time, the structural defects may cause a decrease in breakdown strength for BOPP–AA-10 films.

Many studies demonstrate that the energy loss mechanism for the capacitive films is closely related to the conduction loss at the high electric field and high temperature[29–33]. Electrical conductivity not only reduces discharged energy density and charge-discharge efficiency but also generates joule heat inside the dielectric layers, further lowering the upper limit working temperature. Therefore, to obtain excellent high-temperature resistance performance, it is essential to reduce conduction loss under extreme conditions. The leakage current density of the resultant films is measured at 125 °C and 200 kV/mm, as shown in Figure 4(e) and Figure S5. The results demonstrate that the leakage current density decreases from 1.18×10^{-7} A/cm² of pristine BOPP to 4.09×10^{-8} A/cm² of modified BOPP–AA films. The Schottky fitting can reflect the electric charge injection and is given in Figure 4(f). The increase of the intercept in the fitting line refers to the increase in the barrier height after UV irradiation grafting, which lowers conduction loss at high temperatures[34,35]. The possible mechanism for the improved barrier height is given below. The introduction of the carbonyl group may introduce deep traps, which can capture the charge injected from the metal electrode and restrict the carrier's migration. The trapped charges at the interface can create a local electric field that is opposite to the external electric field. Simulta-

neously, the trapped charges on the surface offer a repulsive force to the injected charges, resulting in lower conduction loss of the BOPP–AA films.

2.4 Structural simulation and trap characteristics

In order to further reveal the mechanism for the suppressed conduction loss at high-temperature, the structural simulation and trap characteristics are well studied[25]. The electron-acceptor C=O groups grafted onto BOPP films will reduce the highest occupied molecular orbital (HOMO) and lowest unoccupied molecular orbital (LUMO). However, the electron-donor O–H groups binding onto BOPP will rise the HOMO and LUMO. The above mentioned factors induce the reduction of the decreased orbital spacing. Figures 5(a) and 5(b) shows the 3-dimensional LUMO and HOMO distributions of BOPP, BOPP–AA, BOPP-dimer, and BOPP–AA-dimer. The energy level shows that the HOMO–LUMO gap in the BOPP and BOPP–AA films are 9.66 eV and 7.18 eV, respectively. The lower LUMO and higher HOMO properties increase the possibility that the injection charges stay in the grafted surface layer rather than migrate into the inner layer. The charge migration path along the molecular chains is represented by energy level distribution. It can be seen that the energy level distribution of pristine BOPP films is almost symmetric and distributed throughout the molecular chain. In contrast, the energy level distribution is asymmetric for the BOPP–AA films, which may make the carriers' migration more difficult and restrict the molecular chain. For example, the distribution of BOPP–AA-dimer energy level is not symmetrical compared to BOPP-dimer, meaning that the carriers' migration along the molecular chain is much more difficult.

The thermally stimulated depolarization current (TSDC) and kelvin probe force microscopy (KPFM) are used to further intuitively prove the existence of charge trap and the electrostatic
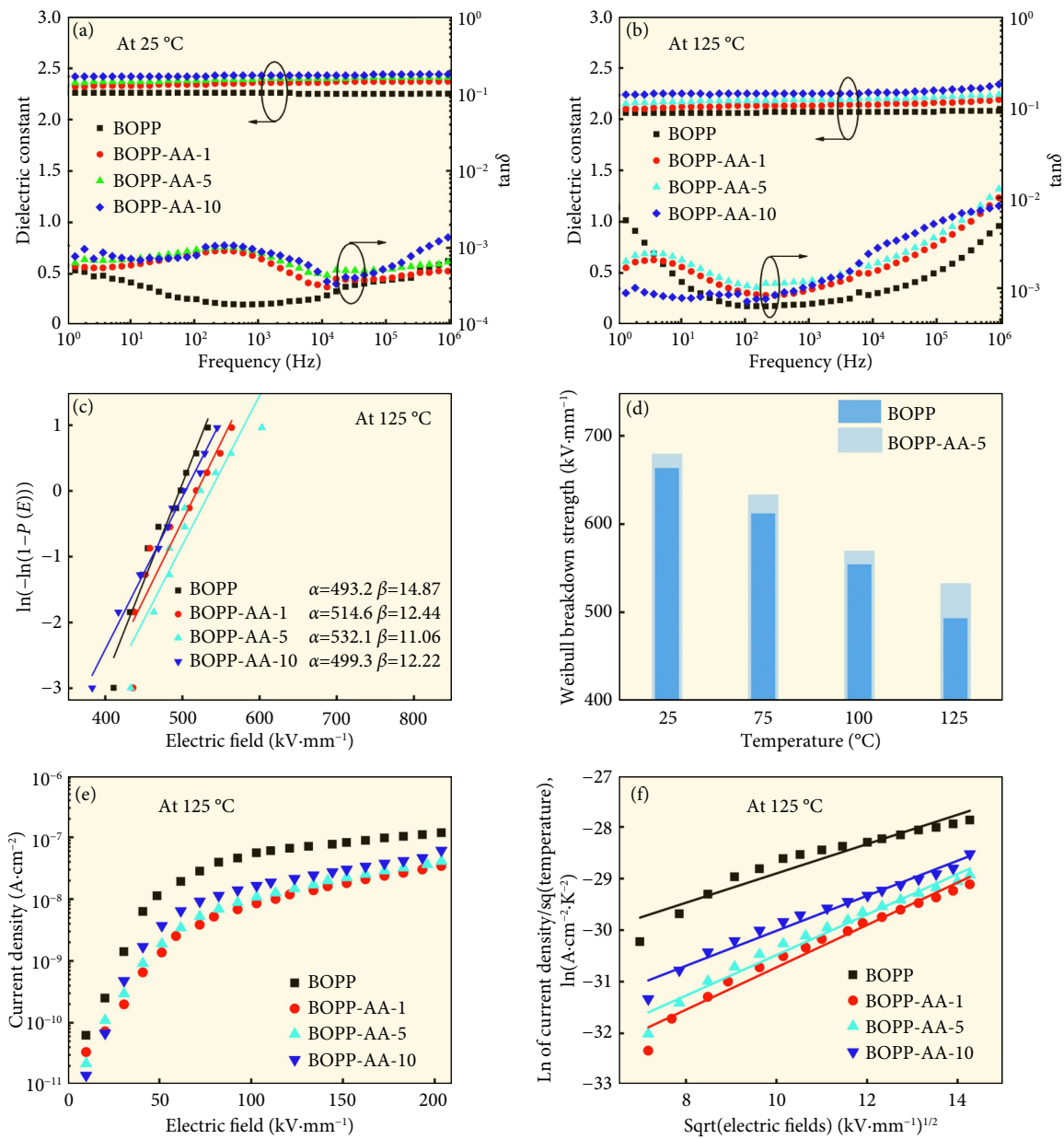
Fig. 4 Dielectric constant and dielectric loss of the BOPP–AA films at **(a)** 25 °C and **(b)** 125 °C. **(c)** Weibull distribution and **(d)** DC breakdown strength. **(e)** Leakage current density and **(f)** Schottky fitting curve.

potential distribution in the BOPP-AA films, respectively, as displayed in Figures 5(c) and 5(d) . The weak peak at −5 °C in TSDC curves refers to the glass transition temperature of BOPP films, whereas the peak at a higher temperature of ~90 °C is attributed to the trapped charges. The peak offset to a much higher temperature indicates the formation of deeper traps[36,37]. From Figure 5(d), it can be seen that the surface electrostatic potential decreases for BOPP-AA films compared to that of pristine BOPP films. For BOPP–AA films, its surface potential decreases to 189 mV (BOPP~ 377 mV), indicating that the grafting modification in the BOPP–AA-5 films is beneficial to capturing an additional negative charge of ~2.8 mC·m⁻². The additional surface charge densities were determined by the equation: $\frac{Q}{A} = \frac{CU}{A} = \frac{\varepsilon_0 \varepsilon_r A U/d}{A} = \frac{\varepsilon_0 \varepsilon_r U}{d}$, where Q is the additional charge, U is the difference of the surface potential, ε_0 is the vacuum dielectric constant (value of 8.85×10^{-12} F·m⁻¹), ε_r is the dielectric constant of BOPP (ε_r~2.2), A is the probe surface areas, and d is

the distance between the probe and the BOPP-AA surface (value of about 3 nm)[15,38,39]. As shown in Figure S6, the Zeta potential drops from −58mV to −79mV at pH = 7, further verifying that the surface of the BOPP–AA films is negatively charged, and the enhancement of the photoluminescence intensity indicates the suppression of charges migration by grafting modification.

2.5 Energy storage properties of the BOPP–AA films

The electric displacement–electric field (D–E), discharge energy density (U_e), and energy efficiency (η) curves were measured at different temperatures, as shown in Figures 6(a)–6(c) and Figure S7. Importantly, the maximum temperature is set as 125 °C, which is beyond the upper limit operating temperature of the pristine capacitor PP films (i.e., 105 °C)[40]. As expected, η of the pristine BOPP falls below 90% as the electric field exceeds 180 kV/mm and falls to 75% at 370 kV/mm. Outstandingly, the BOPP–AA-5 modified films maintain a η of above 90% up to 370 kV/mm. As
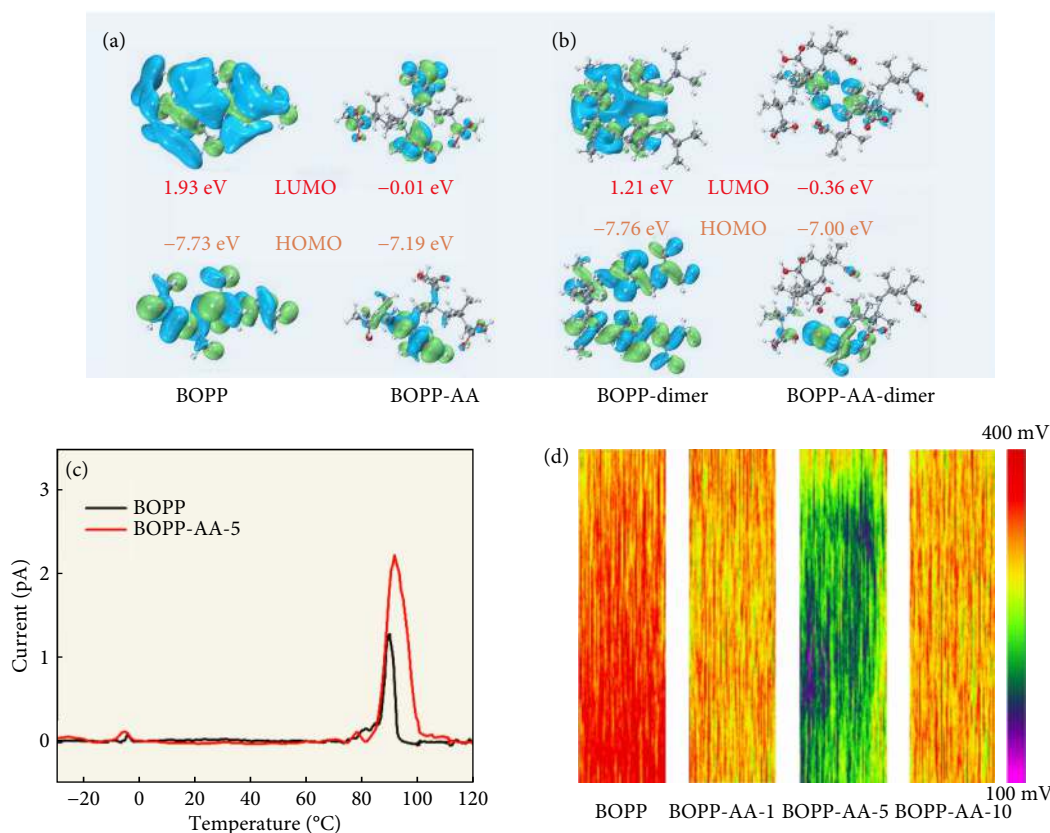
Fig. 5 **(a)** 3D distribution of the LUMO and the HOMO energy levels of BOPP and BOPP–AA. **(b)** BOPP-dimer and BOPP–AA-dimer. **(c)** TSDC of BOPP and BOPP–AA-5. **(d)** KPFM of BOPP–AA films.

shown in Figure 6(d), at 125 °C, the maximum U_e achieved at $\eta >$ 90% for BOPP, BOPP–AA-1, BOPP–AA-5 and BOPP–AA-10 are 0.28, 1.05, 1.32 and 0.61 J/cm³, respectively, indicating that the U_e at $\eta > 90\%$ for BOPP–AA-5 is 474% that of the pristine BOPP.

In order to verify the fatigue resistance of the grafted BOPP-AA films, as shown in Figures 6(e) and 6(f), the fatigue and charge-discharge tests are carried out at 125 °C and 200 kV/mm. BOPP–AA-1 and BOPP–AA-5 show excellent performance under 50,000 cycles, while BOPP–AA-10 electric breaks down after 31,623 cycles, which may be caused by excessive deep trap content, large free charge capture, and electric field distortion in the local area, indicating that the excessive pursuit of trap depth and trap density may be also not a good choice.

3   Conclusions

In this work, the ultraviolet irradiation grafting modification can significantly increase the upper limit operating temperature and enhance the high temperature energy storage performance of BOPP films. The microstructure analyses demonstrate that with the successful grafting modification onto the BOPP film's surface, the dielectric constant of BOPP–AA films shows weak dependence on temperature and frequency, especially its breakdown strength is improved and the leakage current density is suppressed at 125 °C due to the restriction of charge injection. Compared with the pristine BOPP films, the high temperature energy storage performances of BOPP–AA films, including charge and discharge efficiency, discharge energy density, and cycle stability, have been significantly improved. This study proposes an efficient way to enhance the high-temperature energy storage performance of polymer-based capacitor films.

4   Experimental section

4.1   Materials

The materials and reagents used in this experiment are BOPP (PolyK Technologies; 4.8 µm), anhydrous ethanol, AA, methyl acrylate, butyl acrylate, methyl methacrylate (MMA), benzophenone (BP) (Shanghai Macklin Biochemical Co., Ltd.), and acetone (Shanghai Aladdin Biochemical Technology Co., Ltd.). The above materials and chemical reagents are directly used for experimental preparation without further purification.

4.2   Preparation of BOPP–AA films

First, BP particles were dissolved in acetone and stirred for 2 h, after which a homogenous BP acetone solution (2g:100 mL) was produced as the oxidant. AA ethanol solution (2 mol/L) was synthesized by dissolving AA in ethanol for 2 h while stirring. Next, BOPP films were immersed into the abovementioned BP solution for 30 min and transferred into a drying box at 60 °C for 30 min. Thereafter, the BOPP was put in a petri dish poured with a 5 mL AA solution. The grafting reaction was then accelerated by UV irradiation. Herein, the numerals 1, 5, and 10 corresponded to the irradiation times, and the irradiation duration of 3s was designated as BOPP–AA-1, BOPP–AA-5, and BOPP–AA-10, respectively. Finally, the resultant films were washed with acetone to remove the by-products and transferred into a drying box at 60 °C for 2 h. Thus, the BOPP–AA films with UV irradiation grafting modification were successfully prepared. UV irradiation can produce a range of processes, including molecular chain breakage, grafting, cross-linking, and stabilizer denaturation.
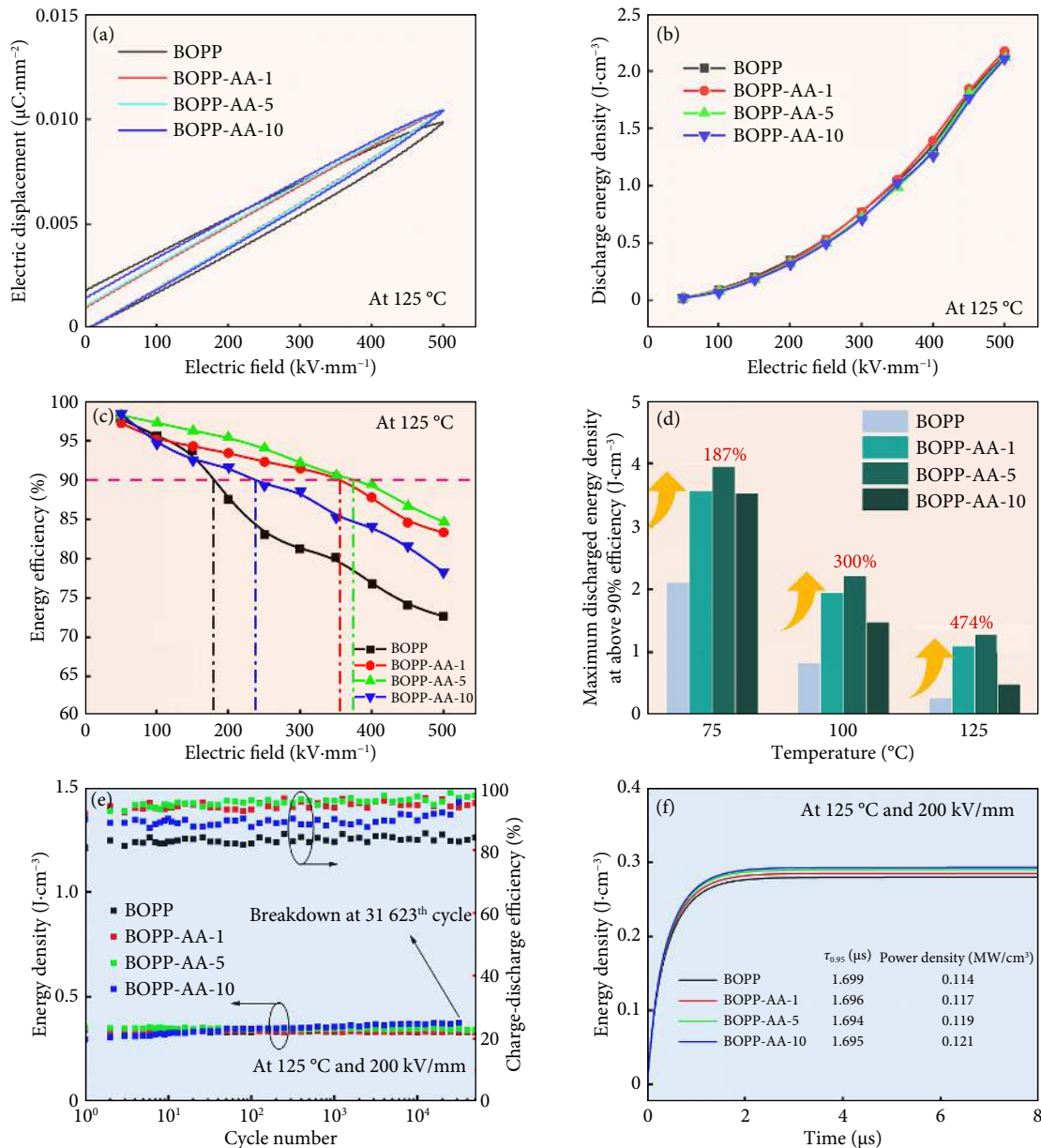
Fig. 6 **(a)** Electric displacement–electric field (*D–E*) loops. **(b)** Charge–discharge efficiency and **(c)** discharged energy density at 125 °C of BOPP–AA films. **(d)** Maximum discharged energy density achieved at above 90% charge-discharge efficiency measured. **(e)** U_e and η obtained from cyclic fast discharge tests of BOPP–AA films. **(f)** The discharged energy density of BOPP–AA films.

4.3 Characterization

The UV light had a power of 3 kW and a wavelength of 365 nm. X-ray diffraction (XRD) patterns of the BOPP–AA films were all tested by the EMPYREAN X-ray diffractometer, which adopted a copper target as the radiation source, and the operating voltage and current were 40 kV and 40 mA, respectively. Fourier Transform infrared spectroscopy (FTIR) (NEXUS 670) and atomic force microscopy (AFM) (Brucker Icon) were used to characterize and analyze the physical structure and the surface properties of the dielectric. The element composition and chemical bonds of the surface were tested by X-ray photoelectron spectroscopy (XPS) with the Thermo Scientific K-Alpha. A contact angle meter (JY-82) was used to measure the water contact angles of BOPP films. Sur-PASS evaluated the surface Zeta potential. Kelvin probe force microscopy (KPFM) in non-contact mode was used to determine the surface potential of the samples. A broadband dielectric spec-

trometer (Novocontrol GmbH, Germany) was employed to measure the dielectric properties. Differential scanning calorimetry (DSC) was performed using a METTLER DSC1 with a constant nitrogen flow rate of 10 mL/min. The BOPP was heated from 25 °C to 200 °C at a heating rate of 4 °C/min, and the weight of the examined samples was 8–10 mg. The molecular weight distribution of the BOPP-AA films was measured by gel permeation chromatography (PL-GPC220). The current density was characterized by a precision LC ferroelectric test system (Radiant Technologies, USA). Furthermore, the DC breakdown test system was used to examine the breakdown strength of thin films, and the cumulative breakdown probability was determined using the Weibull distribution. A modified Sawyer-Tower circuit was used for the cyclic rapid charge-discharge testing. The fast discharge tests were performed through a capacitor charge-discharge test system with a load resistor of 10 kΩ. A steady-state/transient fluo-

rescence spectrometer (Edinburgh FLS1000) was used to measure the photoluminescence intensity of BOPP–AA films. The ferroelectric complete test equipment was used to assess thermally stimulated depolarization current (TSDC). The samples were polarized for 30 min at 80 °C in a 20 kV/mm DC electric field before being abruptly chilled to −40 °C in the same electric field. Afterward, the samples were placed at −40 °C for 5 min, and then the electric field was removed. Finally, the samples were short-circuited and heated to 120 °C at a rate of 4 °C/min while the current was recorded.

Acknowledgements

Article history

Additional information

Supplementary information The online version contains supplementary material available at https://doi.org/10.23919/IEN.2022.0046.

Declaration of competing interest

The authors have no competing interests to declare that are relevant to the content of this article.

References

[1] Ritamäki, M., Rytöluoto, I., Lahti, K. (2009). Performance metrics for a modern BOPP capacitor film. *IEEE Transactions on Dielectrics and Electrical Insulation*, 26: 1229–1237.

[2] Zhang, T. D., Zhao, X. W., Zhang, C. H., Zhang, Y., Zhang, Y. Q., Feng, Y., Chi, Q. G., Chen, Q. G. (2021). Polymer nanocomposites with excellent energy storage performances by utilizing the dielectric properties of inorganic fillers. *Chemical Engineering Journal*, 408: 127314.

[3] Li, S. T., Yin, G. L., Chen, G., Li, J. Y., Bai, S. N., Zhong, L. S., Zhang, Y., Lei, Q. Q. (2010). Short-term breakdown and long-term failure in nanodielectrics: A review. *IEEE Transactions on Dielectrics and Electrical Insulation*, 17: 1523–1535.

[4] Ho, J. S., Greenbaum, S. G. (2018). Polymer capacitor dielectrics for high temperature applications. *ACS Applied Materials & Interfaces*, 10: 29189–29218.

[5] Johnson, R. W., Evans, J. L., Jacobsen, P., Thompson, J. R., Christopher, M. (2004). The changing automotive environment: High-temperature electronics. *IEEE Transactions on Electronics Packaging Manufacturing*, 27: 164–176.

[6] Zhang, T., Yang, L., Zhang, C., Feng, Y., Wang, J., Shen, Z., Chen, Q., Lei, Q., Chi, Q. (2022). Polymer dielectric films exhibiting superior high-temperature capacitive performance by utilizing an inorganic insulation interlayer. *Materials Horizons*, 9: 1273–1282.

[7] Liu, B., Yang, M. H., Zhou, W. Y., Cai, H. W., Zhong, S. L., Zheng,

[8] M. S., Dang, Z. M. (2020). High energy density and discharge efficiency polypropylene nanocomposites for potential high-power capacitor. *Energy Storage Materials*, 27: 443–452.

[8] Feng, M. J., Chi, Q. G., Feng, Y., Zhang, Y., Zhang, T. D., Zhang, C. H., Chen, Q. G., Lei, Q. Q. (2020). High energy storage density and efficiency in aligned nanofiber filled nanocomposites with multilayer structure. *Composites Part B: Engineering*, 198: 108206.

[9] Yao, J., Hu, L., Zhou, M., You, F., Jiang, X., Gao, L., Wang, Q., Sun, Z., Wang, J. (2018). Synergistic enhancement of thermal conductivity and dielectric properties in Al$_2$O$_3$/BaTiO$_3$/PP composites. *Materials*, 11: E1536.

[10] Chi, Q., Zhou, Y., Feng, Y., Cui, Y., Zhang, Y., Zhang, T., Chen, Q. (2020). Excellent energy storage performance of polyetherimide filled by oriented nanofibers with optimized diameters. *Materials Today Energy*, 18: 100516.

[11] Mashhadzadeh, A. H., Fereidoon, A., Ahangari, M. G. (2017). Atomistic modeling of interfacial interaction between polyvinyl chloride and polypropylene with Boron-Nitride monolayer sheet: A density functional theory study. *Superlattices and Microstructures*, 111: 23–31.

[12] Liu, D. Y., Wu, L. Y., Wu, K., Xu, S. M., Sui, G. P., Jing, M. F., Zhao, J., Wei, Y., Fu, Q. (2019). Largely enhanced energy density of polypropylene based nanocomposites via synergistic hybrid fillers and high shear extrusion assisted dispersion. *Composites Part A: Applied Science and Manufacturing*, 119: 134–144.

[13] Feng, Y., Zhou, Y. H., Zhang, T. D., Zhang, C. H., Zhang, Y. Q., Zhang, Y., Chen, Q. G., Chi, Q. G. (2020). Ultrahigh discharge efficiency and excellent energy density in oriented core-shell nanofiber-polyetherimide composites. *Energy Storage Materials*, 25: 180–192.

[14] Pourrahimi, A. M., Kumara, S., Palmieri, F., Yu, L., Lund, A., Hammarström, T., Hagstrand, P. O., Scheblykin, I. G., Fabiani, D., Xu, X., et al. (2021). Repurposing poly(3-hexylthiophene) as a conductivity-reducing additive for polyethylene-based high-voltage insulation. *Advanced Materials*, 33: e2100714.

[15] Zheng, M. S., Zheng, Y. T., Zha, J. W., Yang, Y., Han, P., Wen, Y. Q., Dang, Z. M. (2018). Improved dielectric, tensile and energy storage properties of surface rubberized BaTiO$_3$/polypropylene nanocomposites. *Nano Energy*, 48: 144–151.

[16] Zhou, Y., Li, Q., Dang, B., Yang, Y., Shao, T., Li, H., Hu, J., Zeng, R., He, J., Wang, Q. (2018). A scalable, high-throughput, and environmentally benign approach to polymer dielectrics exhibiting significantly improved capacitive performance at high temperatures. *Advanced Materials*, 30: e1805672.

[17] Yan, Q., Xu, W. Y., Rånby, B. (1991). Photoinitiated crosslinking of low density polyethylene I: Reaction and kinetics. *Polymer Engineering and Science*, 31: 1561–1566.

[18] Qu, B. J., Rånby, B. (1993). Photocross-linking of low-density polyethylene. I. Kinetics and reaction parameters. *Journal of Applied Polymer Science*, 48: 701–709.

[19] Balart, J., Fombuena, V., Boronat, T., Reig, M. J., Balart, R. (2012). Surface modification of polypropylene substrates by UV photografting of methyl methacrylate (MMA) for improved surface wettability. *Journal of Materials Science*, 47: 2375–2383.

[20] Li, H., Feng, X. L., Zhang, K. (2021). Study of the classical cassie theory and Wenzel theory used in nanoscale. *Journal of Bionic Engineering*, 18: 398–408.

[21] Smith, B. C. (2021). The infrared spectra of polymers III: Hydrocarbon polymers. *Spectroscopy*, 36: 22–25.

[22] Dai, S. J., Luo, C., Zhang, C., Wang, H., Zhang, Y., Yuan, L. F. (2021). Determination of small-amount polypropylene in imported recycled polyethylene/polypropylene blends by Fourier transform infrared spectroscopy. *E3S Web of Conferences*, 261: 02067.

[23] Neßlinger, V., Orive, A. G., Meinderink, D., Grundmeier, G. (2022). Combined in situ attenuated total reflection-Fourier transform infrared spectroscopy and single molecule force studies of poly(acrylic acid) at electrolyte/oxide interfaces at acidic pH. *Journal of Colloid and Interface Science*, 615: 563–576.

[24] Pope, C. G. (1997). X-ray diffraction and the Bragg equation. *Journal*

of Chemical Education, 74: 129.

[25] Liu, H. L., du, B. X., Xiao, M., Tanaka, T. (2021). High-temperature performance of dielectric breakdown in BOPP capacitor film based on surface grafting. *IEEE Transactions on Dielectrics and Electrical Insulation*, 28: 1264–1272.

[26] Liu, H. L., du, B. X., Xiao, M. (2021). Improved energy density and charge discharge efficiency of polypropylene capacitor film based on surface grafting. *IEEE Transactions on Dielectrics and Electrical Insulation*, 28: 1539–1546.

[27] Chen, J. Y., Li, B. W., Sun, Y., Zhang, P. X., Shen, Z. H., Zhang, X., Nan, C. W., Zhang, S. J. (2021). Greatly enhanced breakdown strength and energy density in ultraviolet-irradiated polypropylene. *IET Nanodielectrics*, 4: 223–228.

[28] Han, C. C., Zhang, X. H., Chen, D., Ma, Y. H., Zhao, C. W., Yang, W. T. (2020). Enhanced dielectric properties of sandwich-structured biaxially oriented polypropylene by grafting hyper-branched aromatic polyamide as surface layers. *Journal of Applied Polymer Science*, 137: 48990.

[29] Li, Q., Yao, F. Z., Liu, Y., Zhang, G. Z., Wang, H., Wang, Q. (2018). High-temperature dielectric materials for electrical energy storage. *Annual Review of Materials Research*, 48: 219–243.

[30] Li, H., Zhou, Y., Liu, Y., Li, L., Liu, Y., Wang, Q. (2021). Dielectric polymers for high-temperature capacitive energy storage. *Chemical Society Reviews*, 50: 6369–6400.

[31] Liu, G., Feng, Y., Zhang, T. D., Zhang, C. H., Chi, Q. G., Zhang, Y. Q., Zhang, Y., Lei, Q. Q. (2021). High-temperature all-organic energy storage dielectric with the performance of self-adjusting electric field distribution. *Journal of Materials Chemistry A*, 9: 16384–16394.

[32] Zhang, T. D., Yang, L. Y., Ruan, J. Y., Zhang, C. H., Chi, Q. G. (2021). Improved high-temperature energy storage performance of PEI dielectric films by introducing an SiO$_2$ insulating layer. *Macromolecular Materials and Engineering*, 306: 2100514.

[33] Liu, G., Zhang, T. D., Feng, Y., Zhang, Y. Q., Zhang, C. H., Zhang, Y., Wang, X. B., Chi, Q. G., Chen, Q. G., Lei, Q. Q. (2020). Sandwich-structured polymers with electrospun boron nitrides layers as high-temperature energy storage dielectrics. *Chemical Engineering Journal*, 389: 124443.

[34] Pan, H., Zhang, Q. H., Wang, M., Lan, S., Meng, F. Q., Ma, J., Gu, L., Shen, Y., Yu, P., Lin, Y. H., et al. (2018). Enhancements of dielectric and energy storage performances in lead-free films with sandwich architecture. *Journal of the American Ceramic Society*, 102: 936–943.

[35] Zhang, B., Liu, J., Ren, M., Wu, C., Moran, T. J., Zeng, S., Chavez, S. E., Hou, Z., Li, Z., LaChance, A. M., et al. (2021). Reviving the "Schottky" barrier for flexible polymer dielectrics with a superior 2D nanoassembly coating. *Advanced Materials*, 33: e2101374.

[36] Zhou, Y., Yuan, C., Wang, S. J., Zhu, Y. J., Cheng, S., Yang, X., Yang, Y., Hu, J., He, J. L., Li, Q. (2020). Interface-modulated nanocomposites based on polypropylene for high-temperature energy storage. *Energy Storage Materials*, 28: 255–263.

[37] Cheng, L., Liu, W. F., Liu, X. W., Liu, C. M., Li, S. T., Xing, Z. L. (2019). Online degradation of biaxial-orientated polypropylene film from HVDC filter capacitors. *IEEE Transactions on Dielectrics and Electrical Insulation*, 26: 26–33.

[38] Chen, J., Shen, Z. H., Kang, Q., Qian, X. S., Li, S. T., Jiang, P. K., Huang, X. Y. (2022). Chemical adsorption on 2D dielectric nanosheets for matrix free nanocomposites with ultrahigh electrical energy storage. *Science Bulletin*, 67: 609–618.

[39] Cui, Z. Q., Sun, J. X., Niu, X. N., Chen, J. M., Ma, W. L., Chi, L. F. (2016). Photo-generated charge behaviors in all-polymer solar cells studied by Kelvin probe force microscopy. *Organic Electronics*, 39: 38–42.

[40] Rabuffi, M., Picci, G. (2002). Status quo and future prospects for metallized polypropylene energy storage capacitors. *IEEE Transactions on Plasma Science*, 30: 1939–1942.